SCIENTIFIC REPORTS

Improving the electrocatalytic properties of Pd-based catalyst for direct alcohol fuel cells: effect of solid solution

Cuilian Wen[1], Ying Wei[1], Dian Tang[1], Baisheng Sa[1], Teng Zhang[1] & Changxin Chen[1,2]

The tolerance of the electrode against the CO species absorbed upon the surface presents the biggest dilemma of the alcohol fuel cells. Here we report for the first time that the inclusion of $(Zr, Ce)O_2$ solid solution as the supporting material can significantly improve the anti-CO-poisoning as well as the activity of Pd/C catalyst for ethylene glycol electro-oxidation in KOH medium. In particular, the physical origin of the improved electrocatalytic properties has been unraveled by first principle calculations. The 3D stereoscopic Pd cluster on the surface of $(Zr, Ce)O_2$ solid solution leads to weaker Pd-C bonding and smaller CO desorption driving force. These results support that the Pd/ZrO_2-CeO_2/C composite catalyst could be used as a promising effective candidate for direct alcohol fuel cells application.

Direct alcohol fuel cells (DAFCs) have been attracted great attention on their potential application in the portable electronics and automobile industries[1]. Among various liquid fuels, the methanol is volatile and relatively toxic, and ethanol has been recognized as the most suitable fuel as it is a sustainable and carbon-neutral transportation fuel[2]. However, it is difficult to break the C-C bond in ethanol at temperature lower than 100 °C, and the main product of ethanol oxidation reaction is acetate. As such, the electron transfer rate of ethanol in the alkaline DAFCs is only 33%[3, 4]. Ethylene glycol (EG) is a good choice to replace ethanol because the main product of the EG oxidation is oxalate[5, 6], such that the ETR reaches 80%, which is much higher than that of ethanol in the alkaline DAFCs[4]. Also, EG has superior energy density ($7.56 \, kWh \, L^{-1}$), higher boiling point (198 °C) and could be produced from biomass in great quantities[7–9], which makes it as an appealing candidate for fuels cells application.

Pt-based catalysts have been investigated extensively as good electrocatalysts for low temperature fuel cells, especially for its acidic-resistant property[10]. However, compared to Pt electrocatalyst, Pd is more abundant, less expensive, and could promote EG oxidation more efficiently in alkaline media[11, 12]. A lot of efforts have been done to prepare the Pd-base catalysts with high catalytic activity and anti-CO-poisoning for alcohol electro-oxidation. In addition to the alloying approach[11, 13–16], oxide-modified Pd has been reported to be superior to Pd/C catalyst for alcohol oxidation[17–22]. For instance, Li *et al.* reported that the addition MgO into Pd/C catalysts could significantly improve the reaction activity and the poisoning resistance for ethanol electro-oxidation due to the synergistic effect between Pd and MgO[19].

CeO_2 is as a well-known promoter in noble metal-based combustion catalysts. In addition, ZrO_2 is always used as the support of Pt for water-gas shift in low temperature[23–25]. In recent studies, CeO_2[26, 27] and ZrO_2[28–30] have attracted increasing interests as the support of Pt or Pd and showed excellent catalytic activity. The $Ce_xZr_{1-x}O_2$ system has also been investigated because that the thermal stability, redox property and oxygen storage capacity could be improved by the addition of ZrO_2 to CeO_2[31–35]. However, there is few work reported about ZrO_2-CeO_2 mixed oxides as support materials on the EG electrocatalytic performance of Pd/C catalysts in the literatures. This prompts us to carry out an extensive and systematic investigation on this topic, which is of great interest and importance.

[1]College of Materials Science and Engineering, Fuzhou University, Fuzhou, Fujian, 350116, P.R. China. [2]National Key Laboratory of Science and Technology on Micro/Nano Fabrication, Key Laboratory for Thin Film and Microfabrication of the Ministry of Education, Department of Micro/Nano Electronics, School of Electronic Information and Electrical Engineering, Shanghai Jiao Tong University, Shanghai, 200240, P.R. China. Correspondence and requests for materials should be addressed to B.S. (email: bssa@fzu.edu.cn) or T.Z. (email: teng_zhang@fzu.edu.cn) or C.C. (email: chen.c.x@sjtu.edu.cn)

In this study, Pd/C, Pd/ZrO$_2$/C, Pd/CeO$_2$/C and Pd/ZrO$_2$-CeO$_2$/C composite catalysts have been prepared and characterized. The effect of the solid solution of ZrO$_2$-CeO$_2$ binary oxides as support materials on the electrocatalytic performance of Pd-based catalysts has been inverstigated. The physical origin of the good anti-CO-poisoning property of Pd$_4$/ZrO$_2$-CeO$_2$ (111) composite catalyst has been unraveled based on first principle calculations as well.

Results

Structural characterization. The TEM images of different catalysts are shown in Fig. 1a–d. It is clearly that Pd nanoparticles of all catalysts are uniform and monodisperse. The average size of Pd is 4.8 nm for Pd/C, 4.1 nm for Pd/CeO$_2$/C, 4.6 nm for Pd/ZrO$_2$/C, and 4.0 nm for Pd/ZrO$_2$-CeO$_2$/C, respectively, as shown in Fig. 1a–d, consistent with that calculated on XRD data (in Fig. S1). It is noticed that the particle size of Pd changes more significantly with the addition of CeO$_2$ than ZrO$_2$ in this work. Similar results have been reported in Pt catalysts modified by Ce$_{0.6}$Zr$_{0.4}$O$_2$[31, 32].

It is observed that some grains with a d-spacing of 0.227 nm from the HRTEM images of all catalysts in Fig. 1e–h, which is assigned for the (111) plane of cubic Pd. And the d-spacing of some grains is 0.276 nm in Pd/CeO$_2$/C (Fig. 1g), corresponding for the (200) plane of CeO$_2$. While the d-spacing of some grains in Pd/ZrO$_2$-CeO$_2$/C (Fig. 1h) turns out to be 0.274 nm, which is smaller than that of Pd/CeO$_2$/C. This could be related to the replacement of Ce^{4+} ions by Zr^{4+} ions, which results in a shrinking of the lattice volume of the solid. Based on the HRTEM results, one can confirm that the addition of 50% ZrO$_2$ contributes to the formation of (Zr, Ce)O$_2$ solid solution in present work.

XPS was employed to investigate the nature of surface species for the catalysts. Figure 2 shows the XPS spectra of Zr 3d and Ce 3d in different species before and after Pd-loading. It is evident that the binding energy of Zr 3d$_{5/2}$ slightly increases from 182.3 eV for ZrO$_2$/C to 182.5 eV for Pd/ZrO$_2$/C (Fig. 2a); while the binding energy of Ce 3d$_{5/2}$ changes from 883.1 eV for CeO$_2$/C to 883.6 eV for Pd/CeO$_2$/C (Fig. 2b), which reveals the effect of Pd-loading on the electronic structure of Zr 3d or Ce 3d. Similar change in binding energy has been observed in Zr 3d$_{5/2}$ (Zr 3d$_{3/2}$) as well as Ce 3d$_{5/2}$ for ZrO$_2$-CeO$_2$/C after Pd-loading, as shown in Fig. 2c–d. The presence of ZrO$_2$-CeO$_2$ in the vicinity of Pd nanoparticles could be beneficial for the EG and CO oxidation[36].

Moreover, the interaction between Zr and Ce was determined by the XPS analysis. It is found the Zr 3d$_{5/2}$ peak of ZrO$_2$-CeO$_2$/C (Fig. 2c) shifts negatively about 0.1 eV compared to that of ZrO$_2$/C (Fig. 2a), and the Ce 3d$_{5/2}$ peak of ZrO$_2$-CeO$_2$/C (Fig. 2d) shifts negatively about 0.1 eV compared to that of CeO$_2$/C (Fig. 2b). It indicates that there was an electronic interaction between the ZrO$_2$ and CeO$_2$, which could play an important role in catalytic reaction and the activation of both dispersed metal and oxide matrix during electrode process[37]. The electron cloud density of Pd could be changed by ZrO$_2$-CeO$_2$/C supporting, and a synergetic effect could be yielded to improve the catalytic activity of Pd catalyst.

The XPS spectra of Pd 3d in different catalysts are shown in Fig. 3. It shows that the peaks corresponding for Pd 3d$_{5/2}$ (~335.7 eV) and Pd 3d$_{3/2}$ (~341.0 eV) core levels can be ascribed to Pd and PdO$_y$ (0 < y < 2) species, respectively[38, 39]. It is obviously that both Pd metal and PdO$_y$ can be observed on the surface of prepared catalysts. The ratio of Pd: PdO$_y$ is respectively calculated to be 1.2, 1.4, 2.0 and 2.3 for Pd/C, Pd/CeO$_2$/C, Pd/ZrO$_2$/C and Pd/ZrO$_2$-CeO$_2$/C. As reported in the literature[33], CeO$_2$ can act as an oxygen storage reservoir, which gives lattice oxygen to Pd and stabilizes Pd in an oxidized form. Therefore, the increased metallic Pd content can be mainly related to (Zr, Ce)O$_2$ solid solution.

In addition, the binding energy of Pd 3d$_{5/2}$ shifts positively from 335.65 eV for Pd/C to 335.70 eV for Pd/CeO$_2$/C, and to 335.74 eV for Pd/ZrO$_2$-CeO$_2$/C. Combining with the XPS results in Zr 3d, Ce 3d and Pd 3d (in Figs 2 and 3), it can conclude that strong interaction exists between Pd and oxides, especially for the addition of (Zr, Ce)O$_2$ solid solution. Moreover, the atom ratio of Pd: Zr: Ce is measured about 6.49: 0.98: 1.02 for Pd/ZrO$_2$-CeO$_2$/C catalyst, while the values are about 6.51: 1.92: 0 and 6.45: 0: 2.01 for Pd/ZrO$_2$/C and Pd/CeO$_2$/C respectively, indicating that Pd has been sucessfully loaded in the oxide support and the atom ratio of Zr: Ce is nearly 1: 1 for ZrO$_2$-CeO$_2$ solid solution.

Electrochemical activity and stability. Figure 4 shows the cyclic voltammograms of different catalysts in 1 M KOH solution. It is known that the position and size of anodic peak often change with the modification of Pd catalyst. In general, the anodic peak in the potential range between −0.9 and −0.7 V corresponds for the oxidation of the absorbed and adsorbed hydrogen, the peak from −0.6 to −0.4 V is for OH$^-$ adsorption, and the peak at about −0.2 V can be ascribed to Pd oxide formation, respectively. In addition, the cathodic peak ranging from 0.0 to −0.4 V is due to the reduction of Pd oxide, and the peak between -0.6 to −0.8 V relates to the hydrogen adsorption/absorption[40, 41]. The reduction peak current density of PdO is 82 mA mg^{-1} for Pd/ZrO$_2$-CeO$_2$/C composite catalyst, which is significantly larger than other catalysts. This indicates the highest electrochemical activity of Pd/ZrO$_2$-CeO$_2$/C composite catalyst in present work.

Figure 5 shows the cyclic voltammograms of different catalysts in 1 M KOH solution containing 1 M EG. There are two anodic peaks observed in the forward and reverse scans. The oxidation current increases with the potential increasing for EG oxidation in the forward scan, then decreases due to the reduced activity of Pd and CO poisoning[43]. The anodic peak appeared during the reverse scan could correspond to re-oxidation process of the intermediate product of EG[17, 42]. It is noticed that the current density (i_f) of forward anodic peak of Pd/ZrO$_2$-CeO$_2$/C (3700 mA mg^{-1}) is much greater than that of Pd/C (1695 mA mg^{-1}) and Pd/CeO$_2$/C (2448 mA mg^{-1}). This implies that the Pd/ZrO$_2$-CeO$_2$/C composite catalyst has highest catalytic activity for EG electro-oxidation. It has been reported that the positive shifts of Pd 3d$_{5/2}$ peak of Pd-based catalysts indicates the decrease in the 3d electron density of Pd. The Pd with low 3d electron density is not easy to bind with the intermediate, and thus the intermediate coverage on Pd surface can be reduced[43]. Therefore, the highest catalytic activity
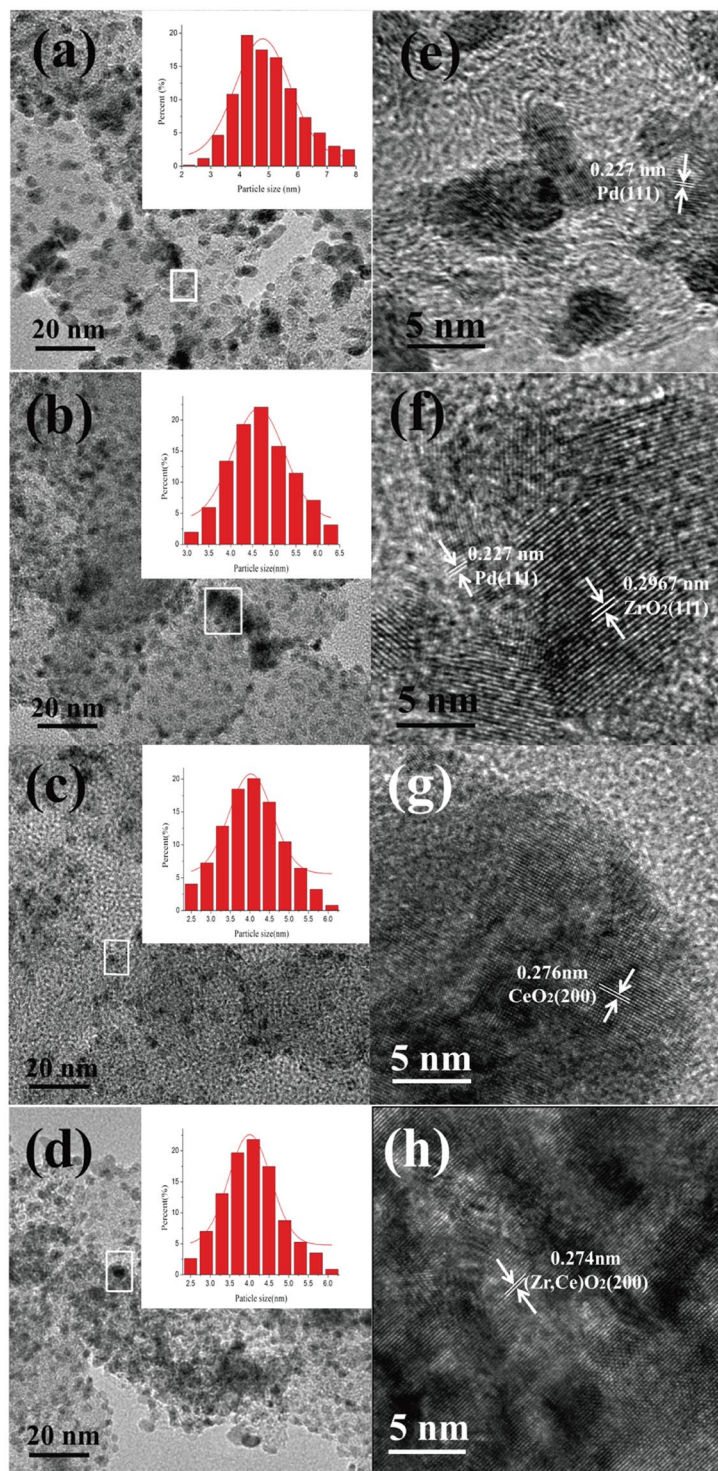
Figure 1. TEM images of different catalysts, for (**a**) Pd/C, (**b**) Pd/ZrO$_2$/C, (**c**) Pd/CeO$_2$/C and (**d**) Pd/ZrO$_2$-CeO$_2$/C. Insets show the corresponding size distribution in (**a,b,c**) and (**d**), respectively. (**e,f,g**) and (**h**) are the HRTEM images for (**a,b,c**) and (**d**), respectively.

of Pd/ZrO$_2$-CeO$_2$/C composite catalyst in present work can be attributed to the interaction between Pd and (Zr, Ce)O$_2$ solid solution (in Figs. 2 and 3) as well as the smallest particle size of Pd (Fig. 1).

Moreover, the chronoamperometry curves of different catalysts were collected in 1 M KOH containing 1 M EG as shown in Fig. 6. It is clear that the Pd/ZrO$_2$-CeO$_2$/C catalyst has a highest initial anodic oxidation current density because of its best electrocatalytic activity in EG. Moreover, there are rapid decays of the current densities observed for all catalysts, due to the formation of CO-like intermediates during EG oxidation[13]. Then the current decreases slowly and reaches a pseudo-steady state after 4000 s. It is worth noting that the Pd/ZrO$_2$-CeO$_2$/C
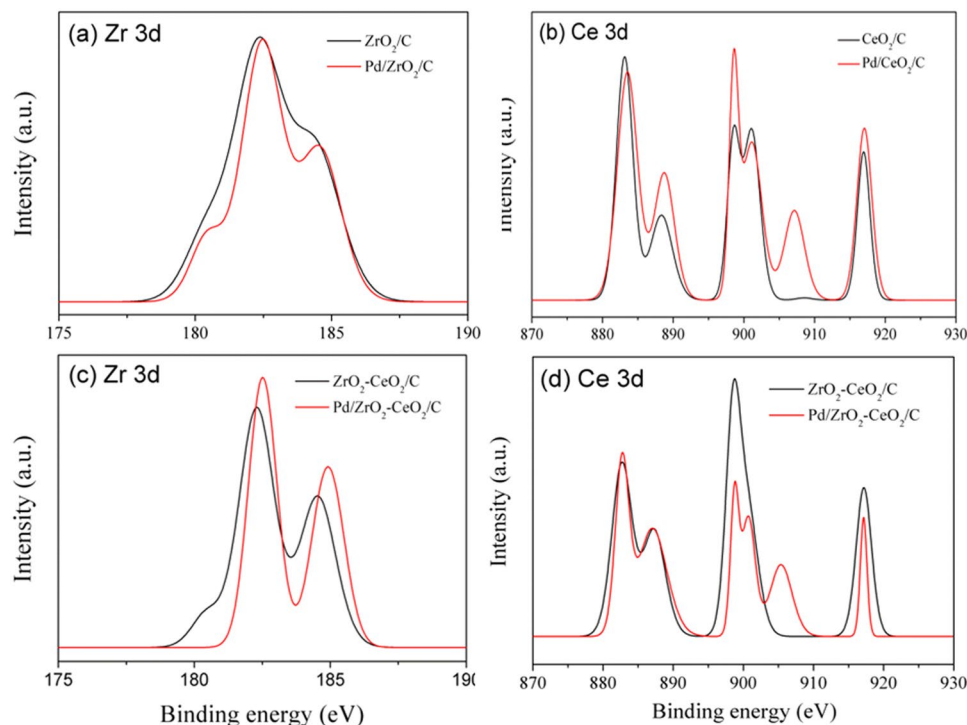
Figure 2. XPS spectra of Zr 3d and Ce 3d in different species before and after Pd-loading, (**a**) Zr 3d for ZrO_2/C and Pd/ZrO_2/C, (**b**) Ce 3d for CeO_2/C and Pd/CeO_2/C, (**c**) Zr 3d and (**d**) Ce 3d for ZrO_2-CeO_2/C and Pd/ZrO_2-CeO_2/C, respectively.
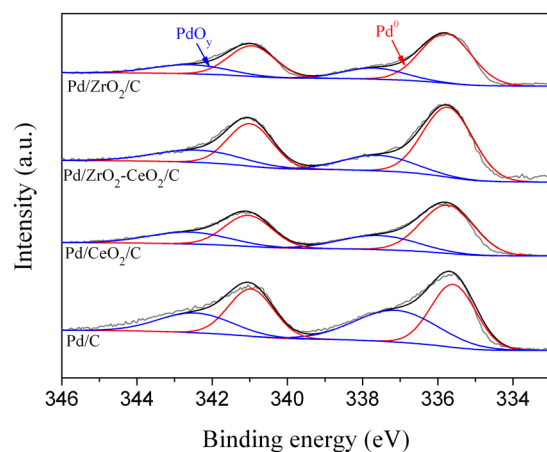
**Figure 3.** XPS spectra of Pd 3d for different catalysts.

composite catalyst exhibits a highest steady state current density during the EG oxidation measurement, indicating its best stability among all catalysts in present work. The current density of Pd/ZrO_2-CeO_2/C catalyst is about 1.7 times as that of Pd/CeO_2/C catalyst (295.5 vs. 177.8 mA. mg^{-1}) after 5000 s.

It is known that CO species are the main poisoning intermediate during the electro-oxidation process, thus a good catalyst for EG electro-oxidation should possess excellent CO electro-oxidizing ability. Figure 7 shows the CO-stripping voltammograms of different catalysts in 1 M KOH. It shows that the CO-striping onset potential of the Pd/ZrO_2-CeO_2/C composite catalyst is similar with all the catalysts studied, and only the peak areas are different, which is related to the electrochemical surface area.

Therefore, the electrochemical active surface area (EAS) is calculated by following equation[44, 45]

$$EAS = Q/mC \qquad (1)$$

where Q is the charge for CO desorption electro-oxidation, m is the amount of Pd loaded, and C ($420\,\mu C\,cm^{-2}$) is the charge needed for the adsorption of a CO monolayer. It is obvious that the EAS of the Pd/ZrO_2-CeO_2/C catalyst is larger than that of Pd/C (117.9 vs. $101.1\,m^2\,g^{-1}$), which further supports the promoted CO-stripping
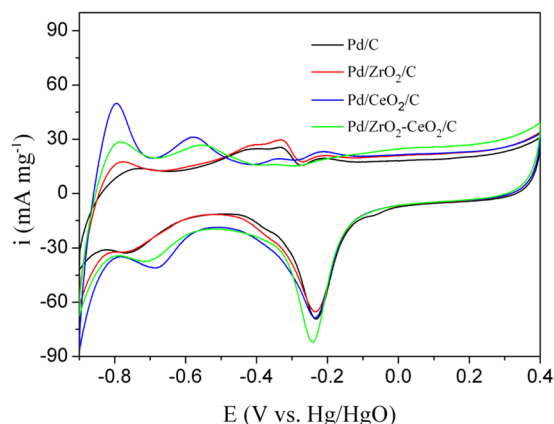
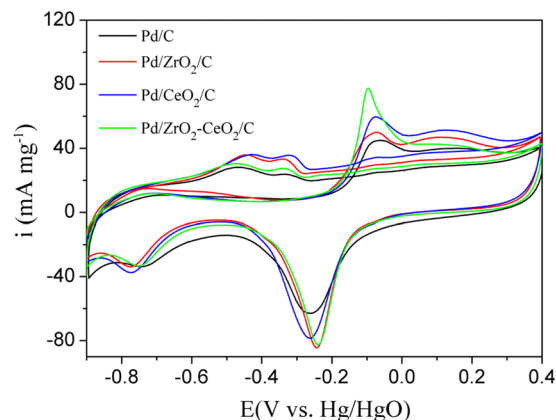**Figure 4.** Cyclic voltammograms of different catalysts in 1 M KOH solution at a scan rate of $50\,mV s^{-1}$.
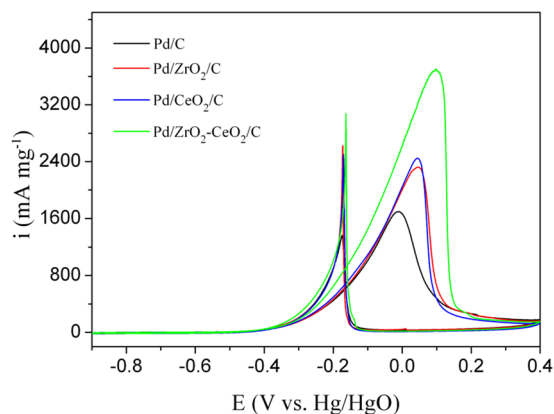
Figure 5. Cyclic voltammograms of different catalysts in 1 M KOH solution containing 1 M EG at a scan rate of $50\,mV s^{-1}$.
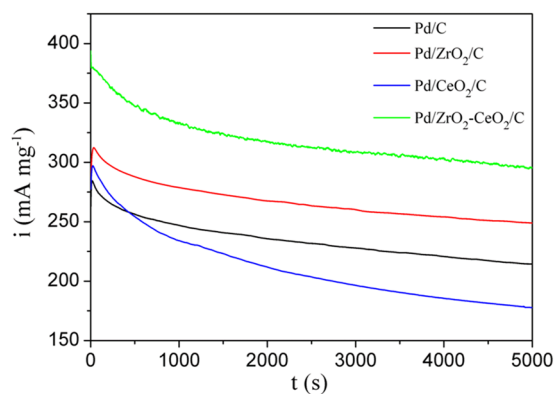
Figure 6. Chronoamperometric curves of different catalysts recorded at $-0.25\,V$ in 1 M KOH solution containing 1 M EG.

of (Zr, Ce)O$_2$ solid solution. To clarify the catalytic effect of ZrO$_2$-CeO$_2$, the specific activity of catalysts has been calculated by normalizing the cyclic voltammograms results (in Fig. 5) to EAS result. It is also worth noting that the specific activity obviously increases from $1.68\,mA\,cm^{-2}$ for Pd/C to $3.14\,mA\,cm^{-2}$ for Pd/ZrO$_2$-CeO$_2$/C catalyst. Therefore, the inclusion of (Zr, Ce)O$_2$ solid solution enhances the stability as well as activity of Pd/C catalyst, which could be related to the strong interaction between Pd and (Zr, Ce)O$_2$ solid solution and the weaker adsorption strength between the Pd surface and CO as discussed for XPS result in Fig. 3.

The TEM images and particle size distribution of different catalysts after 900 cycles in the 1 M KOH solution containing 1 M EG are displayed in Fig. 8. It shows that the average diameter of Pd nanoparticles after 900 cycles

Figure 7. CO-stripping voltammograms of different catalysts in 1 M KOH solution at a scan rate of $50\,\mathrm{mV\,s^{-1}}$.

increases to 6.5, 5.5, 4.9 and 4.5 nm for Pd/C, Pd/ZrO$_2$/C, Pd/CeO$_2$/C and Pd/ZrO$_2$-CeO$_2$/C, respectively. The smaller increasement in diameter of Pd particles for Pd/ZrO$_2$-CeO$_2$/C has been obtained compared with that of catalysts before test as shown in Fig. 1, which indicates its better stability in the alkaline solution. This result can be attributed to protective decoration of Pd/C by (Zr, Ce)O$_2$ solid solution which can prevent Pd from dissolution and agglomeration during cycling[46]. It is also observed that the d-spacing of 0.227 which belongs to the (111) plane of cubic Pd, from the HRTEM images of all catalysts in Fig. 9e–h, and the corresponding d-spacing of ZrO$_2$, CeO$_2$ and ZrO$_2$-CeO$_2$ have been measured and confirmed, which is similar as the TEM analyses of the catalysts before cycling in Fig. 1.

Discussions

It is well established that the addition of oxides into Pd-based catalysts increases alcohol oxidation and the removal of adsorbed CO on the surface of catalysts. The higher catalytic activity of Pd/ZrO$_2$-CeO$_2$/C compared with that of Pd/CeO$_2$/C in present work could be related to the addition of ZrO$_2$ to CeO$_2$. According to the bi-functional mechanism, the addition of ZrO$_2$ probably more easily activates H$_2$O to form oxygen-containing species (OH$_{ads}$) at lower potential. Then the CO-like intermediate species could be reacted with these oxygen-containing species on the surface of Pd surface to release the active sites for further alcohol oxidation[30]. It has also been reported that the synergistic effect can be obtained if intimate mixing (solid solution) is achieved, then the electrochemical properties could be modified[47]. Therefore, the improved electrocatalytic activity and stability of Pd/ZrO$_2$-CeO$_2$/C composite in present work can be mainly attributed to the strong interaction between Pd and (Zr, Ce)O$_2$ solid solution as well as the synergistic effect between CeO$_2$ and ZrO$_2$.

First principle calculations were performed to further unravel the physical origin of the improved electro-catalytic activity and stability of Pd/ZrO$_2$-CeO$_2$/C composite. Since the CeO$_2$ (111) surface is more stable than CeO$_2$(110) surface[48], we have proposed a catalyst model with 3×3 CeO$_2$ p(111) surface slab and a Pd 4-atom cluster, referred to as Pd$_4$/CeO$_2$ (111) hereafter. According to our previously analysis, we have obtained (Zr, Ce)O$_2$ solid solution with CeO$_2$ structure by replacing 50% Ce atoms with Zr atoms. Herein, the special quasi-random structure (SQS) approach[49] has been introduced to model the (Zr, Ce)O$_2$ solid solution. Corresponding catalyst model refers to as Pd$_4$/ZrO$_2$-CeO$_2$ (111) hereafter. Figure 9 illustrates the relaxed structures of Pd$_4$/CeO$_2$ (111) and Pd$_4$/ZrO$_2$-CeO$_2$ (111) catalyst models. Very interestingly, the Pd cluster behaviors is very different on top of the CeO$_2$ and (Zr, Ce)O$_2$ solid solution surface. As can be seen in Fig. 9a, for the Pd$_4$/CeO$_2$ (111) catalyst model, the Pd atoms spread on top of the CeO$_2$ surface, forming a 2D plane structure. On the other hand, the four Pd atoms gather into a tilted tetrahedron on top of the surface of (Zr, Ce)O$_2$ solid solution, forming a 3D stereoscopic cluster in Fig. 9b. The corresponding charge transfer between the Pd$_4$ cluster and oxide surface $\rho_{\mathrm{chargetransfer}}$ illustrated in Fig. 8c and d are analyzed by:

$$\rho_{\mathrm{chargetransfer}} = \rho_{\mathrm{Pd}_4} + \rho_{\mathrm{Oxide}} - \rho_{\mathrm{catalyst}} \tag{2}$$

where ρ_{Pd4}, ρ_{Oxide} and ρ_{catalyst} are the self-consistent charge density of Pd$_4$ clusters CeO$_2$ (111) or ZrO$_2$-CeO$_2$ (111) surface, and Pd$_4$/CeO$_2$ (111) or Pd$_4$/ZrO$_2$-CeO$_2$ (111) catalyst, respectively. As seen, the charge transfer between O and Pd atoms on the CeO$_2$ (111) surface in Fig. 9c is stronger then on the ZrO$_2$-CeO$_2$ (111) surface, indicating that the chemical environment on the ZrO$_2$-CeO$_2$ (111) surface is more homogeneous. We performed the Bader charge[50] analysis to quantify the transfer of charge density. The results show 0.592 e and 0.427 e net charge transferred from the Pd$_4$ cluster to the CeO$_2$ (111) and ZrO$_2$-CeO$_2$ (111) surface, respectively, indicating the 3D stereoscopic cluster is more stable than the 2D plane structure.

We assumed such structure difference leads to different anti-CO-poisoning properties. The required driving forces of CO desorption are evaluated by the following equation:

$$E_{\mathrm{desorption}} = E_{\mathrm{CO}} + E_{\mathrm{catalyst}} - E_{\mathrm{CO/catalyst}} \tag{3}$$

where $E_{\mathrm{CO/catalyst}}$ shows the total energy of Pd$_4$/CeO$_2$ (111) or Pd$_4$/ZrO$_2$-CeO$_2$ (111) catalyst with absorbed CO molecule, E_{catalyst} corresponds to the total energy of Pd$_4$/CeO$_2$ (111) or Pd$_4$/ZrO$_2$-CeO$_2$ (111) catalyst, and E_{CO}
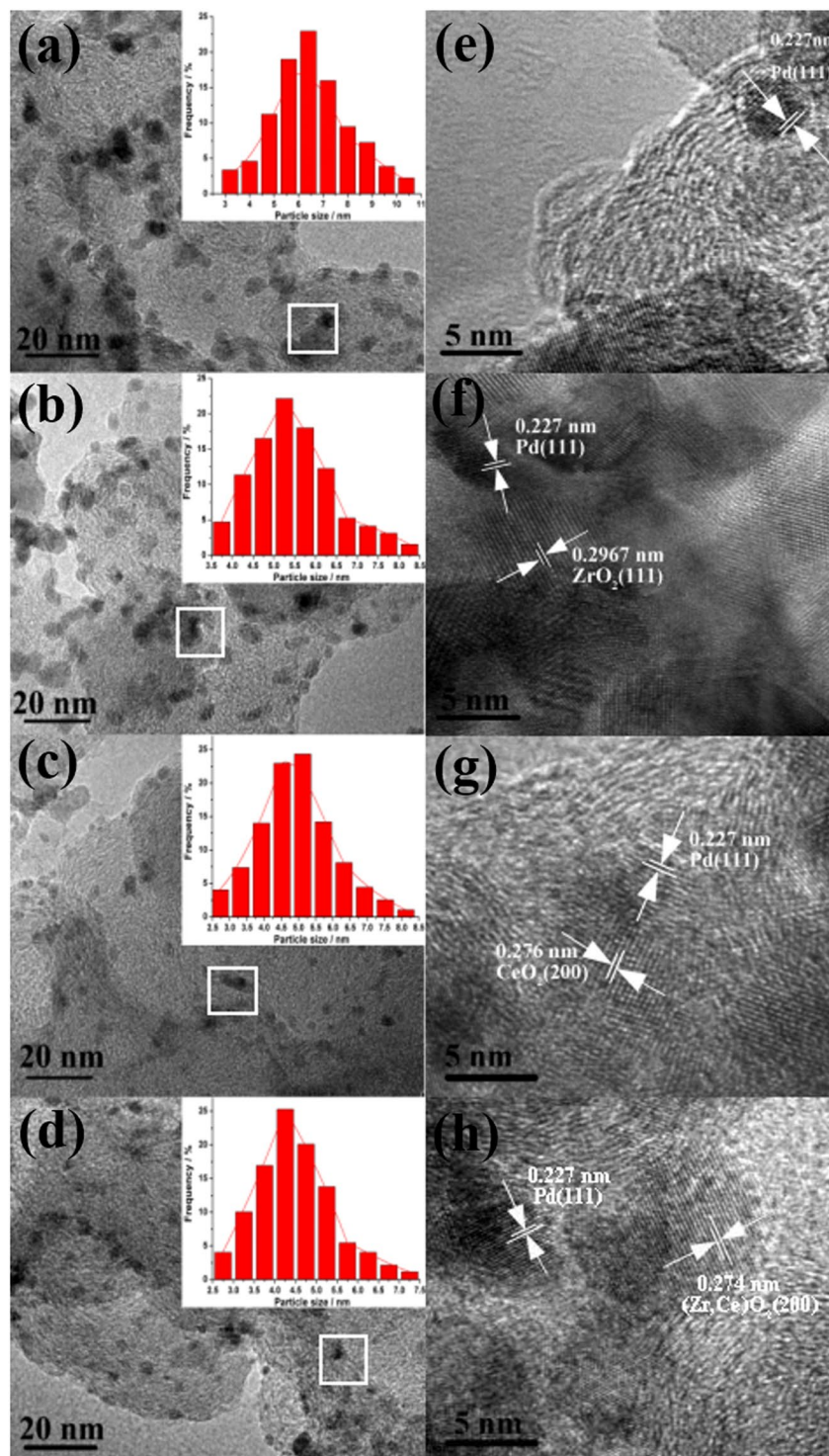
Figure 8. TEM images of different catalysts after 900 cycles in the 1 M KOH solution containing 1 M EG, for (**a**) Pd/C, (**b**) Pd/ZrO$_2$/C, (**c**) Pd/CeO$_2$/C and (**d**) Pd/ZrO$_2$-CeO$_2$/C. Insets show the corresponding size distribution in (**a,b,c**) and (**d**), respectively. (**e,f,g**) and (**h**) are the HRTEM images for (**a,b,c**) and (**d**), respectively.

is the total enegy of CO molecule. The corresponding CO desorption energies for the Pd$_4$/CeO$_2$ (111) and Pd$_4$/ZrO$_2$-CeO$_2$ (111) catalyst are 2.759 eV and 1.836 eV. It is obviously that the desorption of the CO molecule from Pd$_4$/ZrO$_2$-CeO$_2$ (111) catalyst is much easier than that from Pd$_4$/CeO$_2$ (111) catalyst. Hence, the Pd$_4$/ZrO$_2$-CeO$_2$ (111) catalyst presents better anti-CO-poisoning properties, consistent with the best anti-CO-poisoning of the Pd/ZrO$_2$-CeO$_2$/C composite catalyst (in Fig. 7).

To further exploring the anti-CO-poisoning properties, the charge transfers from absorbed CO molecule to Pd cluster was studied by analyzing the charge density differences ρ_{diff}, which is defined as:
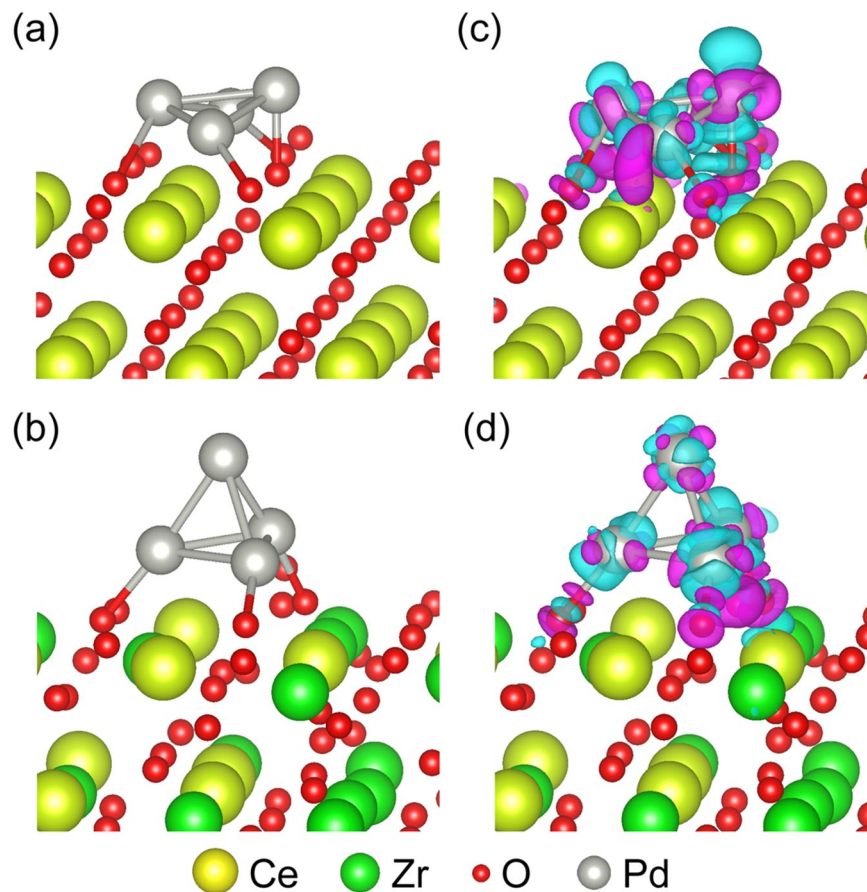
Figure 9. The relaxed (**a**) Pd_4/CeO_2 (111) and (**b**) Pd_4/ZrO_2-CeO_2 (111) catalyst models used to study the CO absorption and desorption mechanism.
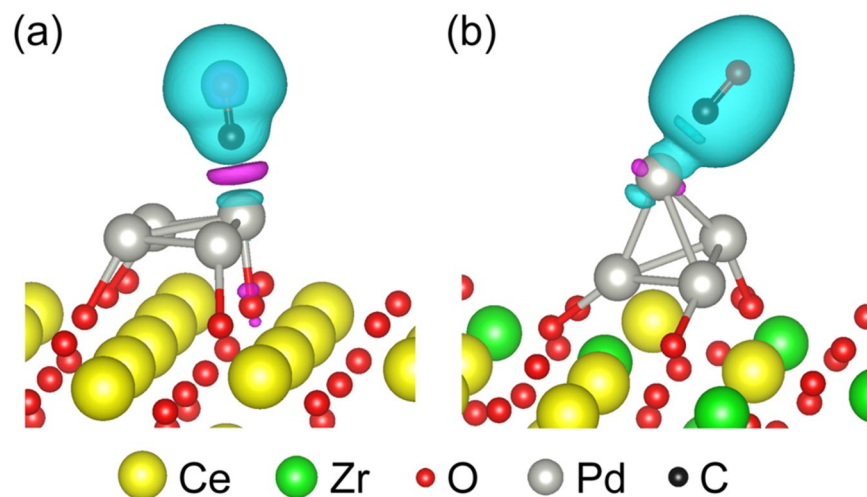
Figure 10. Plots of charge density difference (violet: charge depletion, cyan: charge accumulation) for CO absorbed on top of the (**a**) Pd_4/CeO_2 (111) and (**b**) Pd_4/ZrO_2-CeO_2 (111) catalysts.

$$\rho_{diff} = \rho_{CO/catalyst} - (\rho_{catalyst} + \rho_{CO}) \tag{4}$$

where $\rho_{CO/catalyst}$, $\rho_{catalyst}$ and ρ_{CO} corresponding to the self-consistent charge density of Pd_4/CeO_2 (111) or Pd_4/ZrO_2-CeO_2 (111) catalyst with absorbed CO molecule, Pd_4/CeO_2 (111) or Pd_4/ZrO_2-CeO_2 (111) catalyst, and CO molecule, respectively. Figure 10 plots ρ_{diff} for CO molecule absorbed on Pd_4/CeO_2 (111) and Pd_4/ZrO_2-CeO_2

(111) catalyst. The violet isosurfaces present the charge depletion $\rho_{diff} < 0$, while the cyan isosurfaces show the charge accumulation $\rho_{diff} > 0$. As seen in Fig. 10a, the absorption of CO on top of the Pd_4/CeO_2 (111) catalyst will lead to charge depletion in the middle of the CO molecule and the Pd 2D flat cluster, which contributes to strong Pd-C bonding. Meanwhile, for the case of CO absorbed on the Pd_4/ZrO_2-CeO_2 (111) catalyst as shown in Fig. 10b, the charge accumulation between the CO molecule and the Pd 3D stereoscopic cluster increases the repulsive force between the C and Pd atom, resulting in a weaker Pd-C bonding. Combining with our previously analysis, the 3D stereoscopic Pd cluster on (Zr, Ce)O_2 solid solution contributes to the good anti-CO-poisoning properties of Pd_4/ZrO_2-CeO_2 (111) catalyst.

Conclusions

In present work, the effect of (Zr, Ce)O_2 solid solution on the structures and properties of Pd-based catalysts has been clearly demonstrated. The inclusion of (Zr, Ce)O_2 solid solution reduces the particle size and increases the EAS of Pd nanoparticles, resulting in enhanced electrocatalytic activity of the composite catalyst for EG electro-oxidation in KOH solution. In addition, the strong interaction between Pd and (Zr, Ce)O_2 solution decreases the Pd 3d electron density, which reduces the intermediate coverage on Pd surface and releases more active sites for EG electro-oxidation. The synergistic effect in (Zr, Ce)O_2 also significantly increases the concentration of the OH_{ads} species on Pd surface and thus improves the stability and anti-CO-poisoning of Pd-based composite catalysts. Furthermore, the 3D stereoscopic Pd cluster on the surface of (Zr, Ce)O_2 solid solution were explored based on first principle calculations, which leads to weaker Pd-C bonding and smaller CO desorption driving force. The findings on the good electrocatalytic properties of Pd/ZrO_2-CeO_2/C composite catalyst and the related mechanism will promote the development of stable catalyst for DAFCs application.

Methods

Sample preparation.   26 mg of $CeCl_3 \cdot 7H_2O$ and 1 g urea (Sinopharm Chemical Reagent Co., Ltd, AR) were dissolved in 50 mL of deionized water. 84 mg Vulcan XC-72 carbon black was added into the solution, sonicated for 30 min and magnetic stirred for 1 h. The resulting solution was transferred into the oil bath at 90 °C for 3 h, washed with deionized water after cooling down naturally, and dried at 70 °C. The dried power was heated at 500 °C for 1 h in tube furnace under N_2 atmosphere with a heating rate of 4 °C/min, then cooled down to get the support as CeO_2/C. The ZrO_2/C and ZrO_2-CeO_2/C were also prepared similarly. The molar ratio of $ZrOCl_2 \cdot 8H_2O$ (Sinopharm Chemical Reagent Co., Ltd, AR) to $CeCl_3 \cdot 7H_2O$ is 50:50 for preparing the ZrO_2-CeO_2/C. The mass ratio of the oxide to XC-72 carbon black is 1:7.

The catalysts were prepared through a borohydride reduction approach[43, 51]. 20 mg of $PdCl_2$ (Shanghai Jiuyue Chemical Reagent Co., Ltd, AR) was sonicated in ultrapure water for 2 h. The prepared CeO_2/C was sonicated in ultrapure water for 1 h. Two solutions were then mixed and stirred for 1 h, to obtain a solution with a nominal Pd-loading of 20 wt. %. The pH of this solution was adjusted to 9 using 1 M NaOH. $NaBH_4$ was then added to the solution as a reduction agent, with a molar ratio of 1:8 for Pd and $NaBH_4$. The resulting precipitate was filtered and washed with ultrapure water and ethanol, and then dried at 60 °C. The catalysts are designated as Pd/ZrO_2/C, Pd/ZrO_2-CeO_2/C and Pd/CeO_2/C, respectively. The Pd/C (Pd:C = 20:80 wt.%) was also prepared for comparison.

Materials characterizations.   The high resolution transmission electron microscopy (HRTEM) measurement was conducted in an Electron Microscope system (Tecnai G2 F20 S-TWIN) at 200 kV. Samples were prepared by transferring the catalyst suspension to a copper grid. The catalysts after 900 cycles in 1 M KOH containing 1 M EG were also subjected to TEM measurement.

The electronic structures of Zr 3d and Ce 3d, in different species before and after Pd-loading, were investigated by X-ray photoelectron spectroscopy (ESCALAB 250, Thermo Scientific, Inc.) with a monochromatic Al Kα source (10 mA, 15 kV), respectively. The electronic structure of Pd 3d in different catalysts was also measured by XPS. The spectra were fitted by the Gaussian-Lorentzian method, with a background subtraction by Shirley's method[52].

Electrochemical measurements.   3 mg of catalysts was added in 0.6 mL of Nafion solution (0.5 wt. %) and stirred for 30 min. 4 μL resulting ink was then transferred onto the electrode surface (glassy carbon disk, 3 mm in diameter), and dried at 70 °C for 10 min.

The electrochemical properties of catalysts were measured using an electrochemical workstation (CHI660D, Chenhua Inc., Shanghai, China) in a three-electrode system. The Pt plate (1 cm²) was served as the counter electrode, a Hg/HgO electrode for the reference electrode, and the glassy carbon disk electrode for the working electrode. All measurements were conducted in the water bath of 25 ± 1 °C. The measured Pd loading in the catalysts was 0.057 mg cm⁻², by an inductively coupled plasma equipped with with atomic emission spectroscopy (ICP-AES).

The chronoamperometry was performed at a potential of −0.25 V (1 M KOH containing 1 M EG). In the electrochemical CO-stripping measurements, CO was bubbled into the solution for 15 min with a fixed the catalyst potential (0 V vs. Hg/HgO). The residual CO in the solution was removed by N_2 (99.9%). The cyclic voltammograms (CVs) were conducted in the potential ranging from −0.9 V to 0.4 V vs. Hg/HgO with a sweep rate of 50 mV s⁻¹ (1 M KOH and 1 M KOH containing 1 M EG).

First principle calculations.   Our first principle calculations based on the density functional theory, were performed using the Vienna ab initio simulation package (VASP)[53] in conjunction with the projector augmented wave (PAW) generalized gradient approximations (GGA)[54] of Perdew-Burke-Ernzerhof (PBE)[55] pseudopotentials. The valence electron configurations for C, O, Zr and Ce were $2s^2 2p^2$, $2s^2 2p^4$, $4s^2 4p^6 5s^2 4d^2$ and $5s^2 5p^6 6s^2 4f^1 5d^1$, respectively. The geometry convergence was achieved with the Γ symmetry K-point using the Gaussing smearing ($\sigma = 0.02$ eV) with the cut-off energy of 500 eV. The CeO_2 p(111) surface slab is modeled by a (3 × 3) unit cell. The relaxation convergence for ions and electrons were 1×10^{-5} and 1×10^{-6} eV, respectively. The crystal structures and polyhedrons were visualized using the VESTA tool[56].

References

1. Vigier, F., Coutanceau, C., Perrard, A., Belgsir, E. M. & Lamy, C. Development of anode catalysts for a direct ethanol fuel cell. *Journal of Applied Electrochemistry* **34**, 439–446 (2004).
2. An, L., Zhao, T. S., Zeng, L. & Yan, X. H. Performance of an alkaline direct ethanol fuel cell with hydrogen peroxide as oxidant. *International Journal of Hydrogen Energy* **39**, 2320–2324 (2014).
3. An, L., Chai, Z. H., Zeng, L., Tan, P. & Zhao, T. S. Mathematical modeling of alkaline direct ethanol fuel cells. *International Journal of Hydrogen Energy* **38**, 14067–14075 (2013).
4. An, L. & Chen, R. Recent progress in alkaline direct ethylene glycol fuel cells for sustainable energy production. *Journal of Power Sources* **329**, 484–501 (2016).
5. Antolini, E. & Gonzalez, E. R. Alkaline direct alcohol fuel cells. *Journal of Power Sources* **195**, 3431–3450 (2010).
6. Bianchini, C. & Shen, P. K. Palladium-Based Electrocatalysts for Alcohol Oxidation in Half Cells and in Direct Alcohol Fuel Cells. *Chemical Reviews* **109**, 4183–4206 (2009).
7. Yang, Y. *et al.* Pd nanoparticles supported on phenanthroline modified carbon as high active electrocatalyst for ethylene glycol oxidation. *Electrochimica Acta* **154**, 1–8 (2015).
8. Lin, J.-L., Ren, J., Tian, N., Zhou, Z.-Y. & Sun, S.-G. *In situ* FTIR spectroscopic studies of ethylene glycol electrooxidation on Pd electrode in alkaline solution: The effects of concentration. *Journal of Electroanalytical Chemistry* **688**, 165–171 (2013).
9. Xin, L., Zhang, Z., Qi, J., Chadderdon, D. & Li, W. Electrocatalytic oxidation of ethylene glycol (EG) on supported Pt and Au catalysts in alkaline media: Reaction pathway investigation in three-electrode cell and fuel cell reactors. *Applied Catalysis B: Environmental* **125**, 85–94 (2012).
10. Hong, L., Hao, Y., Yang, Y., Yuan, J. & Niu, L. Synthesis of graphene-supported one-dimensional nanoporous Pt based catalysts, and their enhanced performance on methanol electro-oxidation. *Nanotechnology* **26**, 045604 (2015).
11. Ramulifho, T., Ozoemena, K. I., Modibedi, R. M., Jafta, C. J. & Mathe, M. K. Electrocatalytic oxidation of ethylene glycol at palladium-bimetallic nanocatalysts (PdSn and PdNi) supported on sulfonate-functionalised multi-walled carbon nanotubes. *Journal of Electroanalytical Chemistry* **692**, 26–30 (2013).
12. An, L. & Zhao, T. S. Performance of an alkaline-acid direct ethanol fuel cell. *International Journal of Hydrogen Energy* **36**, 9994–9999 (2011).
13. Du, W. *et al.* Palladium–tin alloyed catalysts for the ethanol oxidation reaction in an alkaline medium. *ACS Catalysis* **2**, 287–297 (2012).
14. Huang, C., Zhang, H., Zhao, Y., Chen, S. & Liu, Z. Diatomite-supported Pd-M (M=Cu, Co, Ni) bimetal nanocatalysts for selective hydrogenation of long-chain aliphatic esters. *Journal of Colloid and Interface Science* **386**, 60–65 (2012).
15. Hinokuma, S., Katsuhara, Y., Ando, E., Ikeue, K. & Machida, M. PdFe/CeO$_2$ bimetal catalysts prepared by dual arc-plasma deposition. *Catalysis Today* **201**, 92–97 (2013).
16. Zhang, Z., Xin, L., Sun, K. & Li, W. Pd–Ni electrocatalysts for efficient ethanol oxidation reaction in alkaline electrolyte. *International Journal of Hydrogen Energy* **36**, 12686–12697 (2011).
17. Ye, K.-H., Zhou, S.-A., Zhu, X.-C., Xu, C.-W. & Shen, P. K. Stability analysis of oxide (CeO$_2$, NiO, Co$_3$O$_4$ and Mn$_3$O$_4$) effect on Pd/C for methanol oxidation in alkaline medium. *Electrochimica Acta* **90**, 108–111 (2013).
18. Xu, C., Shen, Pk & Liu, Y. Ethanol electrooxidation on Pt/C and Pd/C catalysts promoted with oxide. *Journal of Power Sources* **164**, 527–531 (2007).
19. Li, N., Zeng, Y.-X., Chen, S., Xu, C.-W. & Shen, P.-K. Ethanol oxidation on Pd/C enhanced by MgO in alkaline medium. *International Journal of Hydrogen Energy* **39**, 16015–16019 (2014).
20. Zhao, Y., Zhan, L., Tian, J., Nie, S. & Ning, Z. MnO$_2$ modified multi-walled carbon nanotubes supported Pd nanoparticles for methanol electro-oxidation in alkaline media. *International Journal of Hydrogen Energy* **35**, 10522–10526 (2010).
21. Mahendiran, C., Maiyalagan, T., Scott, K. & Gedanken, A. Synthesis of a carbon-coated NiO/MgO core/shell nanocomposite as a Pd electro-catalyst support for ethanol oxidation. *Materials Chemistry and Physics* **128**, 341–347 (2011).
22. Liu, R. *et al.* Preparation of Pd/MnO$_2$-reduced graphene oxide nanocomposite for methanol electro-oxidation in alkaline media. *Electrochemistry Communications* **26**, 63–66 (2013).
23. Pigos, J. M., Brooks, C. J., Jacobs, G. & Davis, B. H. Low temperature water-gas shift: Characterization of Pt-based ZrO$_2$ catalyst promoted with Na discovered by combinatorial methods. *Applied Catalysis A: General* **319**, 47–57 (2007).
24. Hwang, K.-R., Ihm, S.-K., Park, S.-C. & Park, J.-S. Pt/ZrO$_2$ catalyst for a single-stage water-gas shift reaction: Ti addition effect. *International Journal of Hydrogen Energy* **38**, 6044–6051 (2013).
25. Graf, P. O., de Vlieger, D. J. M., Mojet, B. L. & Lefferts, L. New insights in reactivity of hydroxyl groups in water gas shift reaction on Pt/ZrO$_2$. *Journal of Catalysis* **262**, 181–187 (2009).
26. Altamirano-Gutiérrez, A., Fernández, A. M. & Rodríguez Varela, F. J. Preparation and characterization of Pt-CeO$_2$ and Pt-Pd electrocatalysts for the oxygen reduction reaction in the absence and presence of methanol in alkaline medium. *International Journal of Hydrogen Energy* **38**, 12657–12666 (2013).
27. Wang, J. *et al.* Structural designing of Pt-CeO$_2$/CNTs for methanol electro-oxidation. *Journal of Power Sources* **164**, 555–560 (2007).
28. Bai, Y. *et al.* Electrochemical oxidation of ethanol on Pt–ZrO$_2$/C catalyst. *Electrochemistry Communications* **7**, 1087–1090 (2005).
29. Rutkowska, I. A., Koster, M. D., Blanchard, G. J. & Kulesza, P. J. Enhancement of ethanol oxidation at Pt and PtRu nanoparticles dispersed over hybrid zirconia-rhodium supports. *Journal of Power Sources* **272**, 681–688 (2014).
30. Song, H., Qiu, X. & Li, F. Promotion of carbon nanotube-supported Pt catalyst for methanol and ethanol electro-oxidation by ZrO$_2$ in acidic media. *Applied Catalysis A: General* **364**, 1–7 (2009).
31. Bai, Y. *et al.* Electrochemical characterization of Pt-CeO$_2$/C and Pt-Ce$_x$Zr$_{1-x}$O$_2$/C catalysts for ethanol electro-oxidation. *Applied Catalysis B: Environmental* **73**, 144–149 (2007).
32. Chen, L. F. *et al.* Surfactant-controlled synthesis of Pd/Ce$_{0.6}$Zr$_{0.4}$O$_2$ catalyst for NO reduction by CO with excess oxygen. *Applied Surface Science* **243**, 319–328 (2005).
33. Zhang, Q., Zhao, L., Teng, B., Xie, Y. & Yue, L. Pd/Ce$_{0.8}$Zr$_{0.2}$O$_2$/Substrate Monolithic Catalyst for Toluene Catalytic Combustion. *Chinese Journal of Catalysis* **29**, 373–378 (2008).
34. Masui, T., Imadzu, H., Matsuyama, N. & Imanaka, N. Total oxidation of toluene on Pt/CeO$_2$–ZrO$_2$–Bi$_2$O$_3$/γ-Al$_2$O$_3$ catalysts prepared in the presence of polyvinyl pyrrolidone. *Journal of Hazardous Materials* **176**, 1106–1109 (2010).
35. Bekyarova, E., Fornasiero, P., Kašpar, J. & Graziani, M. CO oxidation on Pd/CeO$_2$–ZrO$_2$ catalysts. *Catalysis Today* **45**, 179–183 (1998).
36. Almeida, T. S., Van Wassen, A. R., VanDover, R. B., de Andrade, A. R. & Abruña, H. D. Combinatorial PtSnM (M=Fe, Ni, Ru and Pd) nanoparticle catalyst library toward ethanol electrooxidation. *Journal of Power Sources* **284**, 623–630 (2015).
37. Feng, L. *et al.* Electrocatalytic properties of PdCeO$_x$/C anodic catalyst for formic acid electrooxidation. *International Journal of Hydrogen Energy* **37**, 4812–4818 (2012).
38. Kim, K. S., Gossmann, A. F. & Winograd, N. X-ray photoelectron spectroscopic studies of palladium oxides and the palladium-oxygen electrode. *Analytical Chemistry* **46**, 197–200 (1974).
39. Yang, G., Chen, Y., Zhou, Y., Tang, Y. & Lu, T. Preparation of carbon supported Pd–P catalyst with high content of element phosphorus and its electrocatalytic performance for formic acid oxidation. *Electrochemistry Communications* **12**, 492–495 (2010).
40. Zhang, Q.-L. *et al.* Simple one-pot preparation of Pd-on-Cu nanocrystals supported on reduced graphene oxide for enhanced ethanol electrooxidation. *Electrochimica Acta* **132**, 551–560 (2014).

41. Liang, Z. X., Zhao, T. S., Xu, J. B. & Zhu, L. D. Mechanism study of the ethanol oxidation reaction on palladium in alkaline media. *Electrochimica Acta* **54**, 2203–2208 (2009).
42. Zheng, J.-N. *et al.* A facile general strategy for synthesis of palladium-based bimetallic alloyed nanodendrites with enhanced electrocatalytic performance for methanol and ethylene glycol oxidation. *Journal of Materials Chemistry A* **2**, 12899–12906 (2014).
43. Wen, W., Li, C., Li, W. & Tian, Y. Carbon-supported Pd–Cr electrocatalysts for the electrooxidation of formic acid that demonstrate high activity and stability. *Electrochimica Acta* **109**, 201–206 (2013).
44. Fornasiero, P. *et al.* Rh-Loaded CeO$_2$-ZrO$_2$ Solid-Solutions as Highly Efficient Oxygen Exchangers: Dependence of the Reduction Behavior and the Oxygen Storage Capacity on the Structural-Properties. *Journal of Catalysis* **151**, 168–177 (1995).
45. Cui, R. *et al.* Fabrication of Pd/Mn$_3$O$_4$/plait-like carbon nanocoils catalyst: A highly active catalyst for ethanol electro-oxidation in alkaline media. *Electrochimica Acta* **147**, 778–784 (2014).
46. Huang, Y., Fu, F., Wu, P., Wang, Y. & Yao, J. A bioinspired approach to protectively decorate platinum–carbon for enhanced activity and durability in oxygen reduction. *Journal of Power Sources* **268**, 591–595 (2014).
47. Gaudet, J., Tavares, A. C., Trasatti, S. & Guay, D. Physicochemical Characterization of Mixed RuO$_2$—SnO$_2$ Solid Solutions. *Chemistry of Materials* **17**, 1570–1579 (2005).
48. Skorodumova, N. V., Baudin, M. & Hermansson, K. Surface properties of CeO$_2$ from first principles. *Physical Review B* **69**, 075401 (2004).
49. Zunger, A., Wei, S. H., Ferreira, L. G. & Bernard, J. E. Special quasirandom structures. *Physical Review Letters* **65**, 353–356 (1990).
50. Yu, M. & Trinkle, D. R. Accurate and efficient algorithm for Bader charge integration. *Journal of Chemical Physics* **134**, 064111 (2011).
51. Lu, L. *et al.* New insights into enhanced electrocatalytic performance of carbon supported Pd–Cu catalyst for formic acid oxidation. *Electrochimica Acta* **85**, 187–194 (2012).
52. Sarkar, A., Murugan, A. V. & Manthiram, A. Low cost Pd-W nanoalloy electrocatalysts for oxygen reduction reaction in fuel cells. *Journal of Materials Chemistry* **19**, 159–165 (2009).
53. Hafner, J. Ab-initio simulations of materials using VASP: Density-functional theory and beyond. *Journal of Computational Chemistry* **29**, 2044–2078 (2008).
54. Perdew, J. P. & Wang, Y. Accurate and simple analytic representation of the electron-gas correlation energy. *Physical Review B* **45**, 13244–13249 (1992).
55. Perdew, J. P., Burke, K. & Wang, Y. Generalized gradient approximation for the exchange-correlation hole of a many-electron system. *Physical Review B* **54**, 16533–16539 (1996).
56. Momma, K. & Izumi, F. VESTA 3 for three-dimensional visualization of crystal, volumetric and morphology data. *Journal of Applied Crystallography* **44**, 1272–1276 (2011).

Acknowledgements

Author Contributions

C.W. and Y.W. prepared the samples and tested the properties. B.S. performed the DFT calculations. D.T., T.Z. and C.C. designed the research. C.W., B.S. T.Z. and C.C. analyzed the data. All authors wrote the paper.

Additional Information

Supplementary information accompanies this paper at doi:10.1038/s41598-017-05323-y

Competing Interests: The authors declare that they have no competing interests.

Publisher's note: Springer Nature remains neutral with regard to jurisdictional claims in published maps and institutional affiliations.